Nonlinear refraction and absorption measurements with chirped femtosecond laser pulses: experiments and simulations

J.-K. Wang

Center for Condensed Matter Sciences, National Taiwan University, Taipei, Taiwan

T.-L. Chiu, C.-H. Chi, and C.-K. Sun

Graduate Institute of Electro-Optical Engineering, National Taiwan University, Taipei, Taiwan

Received July 27, 1998; revised manuscript received November 5, 1998

We report an extension of the spectrally resolved two-beam coupling technique to measure the nonlinear intensity index of refraction ($n_2{}^I$) and the two-photon absorption coefficient (β) by use of chirped laser pulses. The linear chirp parameter b is incorporated into the derivation of a more general model than the previous one [Opt. Lett. **22**, 1077 (1997)]. We have also analyzed the validity of this linear chirp model through a comparison of the experimental results for fused silica with the numerically accurate calculation that considers higher-order chirps obtained by second-harmonic generation frequency-resolved optical gating. The results show that this method potentially can be used to extract the chirp. Finally, we applied this transient spectrally resolved nonlinear transmittance spectroscopy to semiconductor-doped glasses to extract their $n_2{}^I$ and β.
 [S0740-3224(99)00804-8]
OCIS codes: 190.7110, 320.7100, 320.7110, 320.1590.

1. INTRODUCTION

In media with inversion symmetry (such as gases, liquids, and noncrystalline materials), third-order optical nonlinearity is the lowest-order nonlinearity allowed under the electric-dipole approximation. Third-harmonic generation, phase conjugation, saturation, self-focusing, the optical Kerr effect, and two-photon absorption can all be attributed to this optical nonlinearity. There has been a great deal of research directed to investigating these phenomena in various materials and in pursuing their application.[1] The nonlinear intensity index of refraction $n_2{}^I$ and the two-photon absorption coefficient β are normally used to quantitatively characterize these kinds of self-action nonlinear optical behavior. The dependence of $n_2{}^I$ and β on the third-order nonlinear optical susceptibility $\chi^{(3)}$ are given by $n_2{}^I = (3/4\epsilon_0 c n_0{}^2)\mathrm{Re}[\chi_{1111}{}^{(3)}]$ and $\beta = (3k_0/2\epsilon_0 c n_0{}^2)\mathrm{Im}[\chi_{1111}{}^{(3)}]$, respectively.[1] Many experimental techniques have been developed to measure the magnitude and the dynamics of third-order optical nonlinearities. The three most commonly used methods are four-wave mixing, optical-heterodyne-detected optical Kerr gating, and beam distortion measurements (Z scan).[1] The first two methods directly measure the third-order nonlinear susceptibility and usually involve a complicated experimental setup. The third method utilizes the self-focusing effect on the beam's propagation property to measure the nonlinear refractive index. The most commonly used method to extract β, on the other hand, is, the nonlinear transmittance method, which measures the transmittance of the laser beam through the medium as a function of the laser's intensity.

Among these three methods for measuring $\chi^{(3)}$, the Z-scan technique is the simplest and deserves the most discussion.[2] It measures the transmission change in a single focused laser beam through an aperture as a function of the relative positions of the beam's focal position and the sample. Because of the intensity-induced change in the refractive index, a peak-and-valley feature shows up in the transmission measurement. A well-defined beam profile is a necessity for extraction of the real and the imaginary parts of $\chi^{(3)}$. This method has been applied successfully to many materials. However, the Z-scan technique has two major limitations. First, it is relatively insensitive. It thus requires a high laser power density, leading to the possibility of other side effects such as laser-induced damage and other higher-order optical nonlinearities. It is thus more often applied to thick samples to accumulate a larger effect for observation. Second, because the beam spot on the sample during the measurement varies, nonuniform samples may cause serious scattering, which will affect this transmission measurement.

Recently Kang *et al.* demonstrated a new method for measuring both $n_2{}^I$ and β.[3] It relies on two-beam coupling between the pump and the probe pulses. The phase change (cross-phase modulation) and the energy loss (two-photon absorption) of the probe beam caused by the pump beam vary the transmission of the probe beam at a wavelength away from its central wavelength. An analytical model of the normalized transmittance variation based on transform-limited pulses was derived and used to fit the experimental results on fused silica and CdS samples. Nonlinear phase shifts as small as $\sim 10^{-6}$ rad and two-photon absorption coefficients as

small as 10^{-4} cm/GW have been demonstrated. It is a highly sensitive technique for measuring the two nonlinear optical constants.

To extend the use of this sensitive technique, we present here our theoretical and experimental studies of this method with chirped femtosecond laser pulses. In Section 2 we describe the derivation of the analytical linear-chirp model with linearly chirped Gaussian laser pulses. In Section 3 we arrive at a fundamental understanding of the chirp-free and linear-chirp models through the simulation results. The experimental setup for the two-beam coupling method and the frequency-resolved optical gating (FROG) apparatus are given in Section 4. Our experimental results and their comparison with the theoretical simulations are presented and discussed in Section 5. Section 6 concludes the paper.

2. THEORY

For an intense pump pulse copropagating with a weak probe pulse in a nonlinear medium with only third-order optical nonlinearity $\chi^{(3)}$, the equations that describe the nonlinear interactions (nonlinear refraction and two-photon absorption) between the strong pump and the weak probe beams are

$$\frac{\partial I_{\mathrm{pu}}}{\partial z} + \frac{1}{v_g}\frac{\partial I_{\mathrm{pu}}}{\partial t} = -(\alpha + \beta I_{\mathrm{pu}})I_{\mathrm{pu}}, \tag{1}$$

$$\frac{\partial \phi_{\mathrm{pu}}}{\partial z} + \frac{1}{v_g}\frac{\partial \phi_{\mathrm{pu}}}{\partial t} = -kn_2{}^I I_{\mathrm{pu}}, \tag{2}$$

$$\frac{\partial I_{\mathrm{pr}}}{\partial z} + \frac{1}{v_g}\frac{\partial I_{\mathrm{pr}}}{\partial t} = -(\alpha + 2\beta I_{\mathrm{pu}})I_{\mathrm{pr}}, \tag{3}$$

$$\frac{\partial \phi_{\mathrm{pr}}}{\partial z} + \frac{1}{v_g}\frac{\partial \phi_{\mathrm{pr}}}{\partial t} = -2kn_2{}^I I_{\mathrm{pu}}. \tag{4}$$

I_{pr} (I_{pu}) is the intensity of the temporal envelope of the probe (pump) beam, ϕ_{pr} (ϕ_{pu}) is the phase of the probe (pump) beam, α is the linear absorption coefficient, v_g is the group velocity, $k = 2\pi/\lambda$, where λ is the wavelength in vacuum, and $n_2{}^I$ is the nonlinear intensity index of refraction. The slowly varying envelope approximation is assumed and group-velocity dispersion (GVD) is neglected in the derivation of Eqs. (1)–(4). The former approximation is valid when the spectral width of the pulse is much smaller than its central frequency, as it normally is for typical femtosecond laser pulses. Ignoring GVD can be justified only when the dispersion length ($L_D = \tau^2/k''$) is greater than the nonlinear length ($L_{\mathrm{NL}} = \xi_0/n_2{}^I I_{\mathrm{pu}}$), where $k'' = d^2k/d\omega^2$, $\xi_0 = \phi_p c/n_0\omega_0$, and ϕ_p is the peak phase shift induced in the measurement ($\sim 10^{-3}$ rad). For a 100-fs laser pulse ($\tau = 85$ fs) at 800 nm propagating in fused silica ($k'' = 0.0362$ ps^2/m at 800 nm), the dispersion length is $\sim$20 cm. Inasmuch as $n_2{}^I = 2.2 \times 10^{-20}$ m^2/W for fused silica, the nonlinear length is $\sim$4 mm for $I_{\mathrm{pu}} = 10^{12}$ W/m^2, which is the typical peak power density achieved by focusing of femtosecond mode-locked laser pulses. Because the sample thickness L selected for experiments is $\sim$3 mm, both L and L_{NL} are much shorter than L_{D}, and the GVD of the sample can be neglected in the analysis.

Assuming a transform-limited laser pulse, $E(t) \sim \exp(-t^2/\tau^2)$, Kang *et al.* derived the nonlinear transmittance of the probe beam as a function of the time delay Δt between the pump and the probe pulses and the detection detuning $\delta = \omega - \omega_0$ between the central frequency of the laser ω_0 and the detecting frequency[3]:

$$\frac{\Delta T}{T}(\Delta t, \delta) = \frac{2}{\sqrt{3}}\exp(\delta^2\tau^2/6)\exp[-2(\Delta t)^2/3\tau^2] \times [2\Delta\Phi \sin(2\delta\Delta t/3) - q\cos(2\delta\Delta t/3)], \tag{5}$$

where $\Delta\Phi = kn_2{}^I I_{\mathrm{pu}}{}^0 L$, $q = \beta I_{\mathrm{pu}}{}^0 L$, $I_{\mathrm{pu}}{}^0$ is the peak intensity of the pump pulse, and L is the interaction length. In the derivation, both $\Delta\Phi$ and q are assumed to be less than $\sim$0.1 and linear absorption in the medium is neglected. Furthermore, the pump pulse is assumed to be invariant while it is propagating in the medium. Equation (5) can be considered a Gaussian envelope modulated at a radial frequency of $2\delta/3$. The effect of the two-photon absorption is simply a phase shift of this modulation.

The chirp in femtosecond laser pulses is in normally produced laser pulses at the direct output of the mode-locked laser owing to uncompensated GVD in the laser cavity,[4] although chirp-free laser pulses can be achieved with extracavity dispersion compensation with a prism sequence. In performing the spectrally resolved two-beam coupling measurement, one therefore cannot apply the simple model of Kang *et al.*[3] to the cases with chirped laser pulses. Here, for the first time to our knowledge, we derive analytically a more general nonlinear transmittance model with the inclusion of linear chirp. When a linearly chirped pulse is assumed,

$$E(t) = E^0 \exp(-t^2/\tau^2 + ibt^2 + i\omega_0 t), \tag{6}$$

where b is the linear chirp parameter. Because a specific spectral component of the probe pulse after it interacts with the pump pulse is selected for detection, the following derivation is given in the frequency domain. According to the nonlinear wave propagation equations for the probe beam [Eqs. (3) and (4)], the probe electric field after it interacts with the pump pulse in the medium is given by

$$\begin{aligned} E_{\mathrm{pr}}(z = L, \omega) &= \mathrm{FT}[E_{\mathrm{pr}}(z = L, t - \Delta t)] \\ &= \mathrm{FT}\Big\{E_{\mathrm{pr}}(z = 0, t - \Delta t) \\ &\quad \times \exp\Big[-i2\frac{\omega_0}{c}n_0 n_2{}^I L I_{\mathrm{pu}}(t) - \beta L I_{\mathrm{pu}}(t)\Big] \\ &\approx \mathrm{FT}\Big\{E_{\mathrm{pr}}(z = 0, t - \Delta t)\Big[1 - i2\Delta\Phi \\ &\quad \times \exp\Big(-2\frac{t^2}{\tau^2}\Big) - q\exp\Big(-2\frac{t^2}{\tau^2}\Big)\Big]\Big\} \\ &= \mathrm{FT}[E_{\mathrm{pr}}(z = 0, t - \Delta\tau)] \\ &\quad + \mathrm{FT}[\Delta E_{\mathrm{pr}}(z = L, t - \Delta t)], \end{aligned} \tag{7}$$

where $\Delta\Phi$ and q are defined as above, Δt is again the time delay between the pump and the probe pulses, and FT

represents the Fourier transformation from the time domain to the frequency domain. Here we also assume that both nonlinearity parameters are small such that the expansion in Eq. (7) extends only to the first-order term. The nonlinear transmittance change of the probe pulse can be written as

$$\begin{aligned}\frac{\Delta T}{T}(\omega) &= \frac{|E_{\mathrm{pr}}(z=L,\omega)|^2 - |E_{\mathrm{pr}}(z=0,\omega)|^2}{|E_{\mathrm{pr}}(z=0,\omega)|^2} \\ &= \frac{|E_{\mathrm{pr}}(z=0,\omega) + \Delta E_{\mathrm{pr}}|^2 - |E_{\mathrm{pr}}(z=0,\omega)|^2}{|E_{\mathrm{pr}}(z=0,\omega)|^2} \\ &\approx 2\,\mathrm{Re}\frac{\Delta E_{\mathrm{pr}}}{E_{\mathrm{pr}}(z=0,\omega)} \\ &= 2\,\mathrm{Re}\frac{\mathrm{FT}[\Delta E_{\mathrm{pr}}(z=L,t-\Delta t)]}{\mathrm{FT}[E_{\mathrm{pr}}(z=0,t)]},\end{aligned} \tag{8}$$

where $\Delta E_{\mathrm{pr}} \ll E_{\mathrm{pr}}(z=0,\omega)$ is assumed. After some derivation,

$$E_{\mathrm{pr}}(z=0,\omega) = E_{\mathrm{pr}}{}^0\left(\frac{\pi\tau^2}{1-ib\tau^2}\right)^{1/2}\exp\left[-\frac{\delta^2\tau^2}{4(1-ib\tau^2)}\right]. \tag{9}$$

In addition, ΔE_{pr} can be given by

$$\begin{aligned}&\mathrm{FT}[\Delta E_{\mathrm{pr}}(z=L,t-\Delta t)] \\ &\quad = E_{\mathrm{pr}}{}^0(i2\Delta\Phi + q)\left(\frac{\pi\tau^2}{3-ib\tau^2}\right)^{1/2} \\ &\qquad \times \exp\left[\frac{(4\Delta t + i\delta\tau^2)^2}{4\tau^2(3-ib\tau^2)} - 2\frac{(\Delta t)^2}{\tau^2}\right].\end{aligned} \tag{10}$$

Finally, after some algebra, the normalized transmittance change of the probe pulse can be written as

$$\begin{aligned}\frac{\Delta T}{T}(\Delta t,\delta) &= 2\left[\frac{(3+b^2\tau^4)^2 + 4b^2\tau^4}{(9+b^2\tau^4)^2}\right]^{1/4} \\ &\quad \times \exp[g(b,\delta,\tau)] \\ &\quad \times \exp\left\{-\frac{[(\Delta t) - T_s(b,\delta,\tau)]^2}{[\Gamma(b,\tau)]^2}\right\} \\ &\quad \times (2\Delta\Phi\sin\Theta - q\cos\Theta),\end{aligned} \tag{11a}$$

where

$$T_s = \frac{-\delta b\tau^4}{2(3+b^2\tau^4)}, \tag{11b}$$

$$\Gamma = \tau\left[\frac{9+b^2\tau^4}{2(3+b^2\tau^4)}\right]^{1/2}, \tag{11c}$$

$$g = \frac{\delta^2\tau^2}{2(1+b^2\tau^4)(3+b^2\tau^4)}, \tag{11d}$$

and

$$\Theta = \frac{4b}{9+b^2\tau^4}\left(\Delta t + \frac{3\delta}{4b}\right)^2 - \frac{\delta^2}{4b(1+b^2\tau^4)} - \frac{1}{2}\tan^{-1}\left(\frac{2b\tau^2}{3+b^2\tau^4}\right). \tag{11e}$$

Equation (11a) is similar to Eq. (5), whereas the envelope function has a time shift $T_S(b,\delta,\tau)$ that is linearly proportional to δ. Its width parameter Γ depends only on b and τ. The time-delay dependence on the sinusoidal modulation function is, however, much more complicated, and the time shift is also different. The second-order dependence of this time-delay dependence indicates that the modulation in the observed transient must have a chirp. This complication is caused by the linear chirp parameter in the phase of the probe pulse. From the complicated equations (11), we expect that the transient nonlinear transmittance performed with non-transform-limited laser pulses will be different from the one with unchirped pulses. According to Eqs. (11), chirp parameter b is nonnegligible when $b\tau^2 \sim 1$, corresponding to a time–bandwidth product 1.4 times that of a transform-limited Gaussian laser pulse. This is not unusual for 100-fs laser pulses directly from a mode-locked Ti:sapphire oscillator. Finally, for $b = 0$, Eq. (11a) can easily be reduced to Eq. (5).

Apparently, the linear chirp model is still too simplified. It is, however, not feasible to derive a complete analytical solution to include the effect of higher-order chirps. To further explore the effects of the higher-order chirps in the nonlinear transmittance measurement we have thus developed a computer program to perform accurate simulations. The generalized electric field is represented as

$$E(t) = E_{\mathrm{pr}}{}^0\exp\left(-\frac{t^2}{\tau^2}\right)\exp(i\omega_0 t)\exp[i\phi(t)], \tag{12}$$

where $\phi(t)$ is the total phase, which can be obtained from the FROG measurements.[5] Furthermore, the dispersion of material was again neglected in this simulation. With these two assumptions, the program calculates the nonlinear transmittance data,

$$\frac{\Delta T}{T}(\omega,\Delta t) = \frac{|E_{\mathrm{pr}}(z=L,\omega,\Delta t)|^2 - |E_{\mathrm{pr}}(z=0,\omega)|^2}{|E_{\mathrm{pr}}(z=0,\omega)|^2}, \tag{13}$$

by substituting Eq. (12) into Eq. (13). There is no approximation similar to Eqs. (7) and (8) in the calculation. This accurate simulation can thus verify the error in the linear chirp model. Here we adopt a Gaussian envelope function in Eq. (12) for the purpose of comparison with the analytical result obtained with the linear chirp [Eq. (11a)]. Although Ti:sapphire lasers do not necessarily emit Gaussian pulses, the Gaussian fitting to the extracted intensity data from the FROG measurement is very satisfactory, as shown in Fig. 7 below. Finally, utilizing the extracted nonlinear phase variation in the laser pulses from the FROG result, we can then compare the experimental data with the prediction made by this program. An analysis of these data is made in Section 4.

3. SIMULATIONS: CHIRP-FREE AND LINEAR-CHIRP MODELS

In this section we first present the chirp-free model, the case in which no chirp is involved in the calculation, to help in a fundamental comprehension of the experimental results in the technique. The sophisticated nonlinear formula of the linear-chirp model is discussed subsequently to illustrate the importance of linear chirp.

A. Chirp-Free Model

The analytical solution of the two-beam coupling equations for chirp-free laser pulses has been derived [Eq. (5)]. The resultant formula can be understood as the product of two parts:

$$\frac{\Delta T}{T}(\Delta t, \delta) = f(\delta, \tau, \Delta t)\zeta(\delta, \Delta t, \Delta\Phi, q), \tag{14a}$$

with

$$f(\delta, \tau, \Delta t) = \frac{2}{\sqrt{3}}\exp\left(\frac{\delta^2\tau^2}{6}\right)\exp\left(-\frac{2\Delta t^2}{3\tau^2}\right), \tag{14b}$$

$$\zeta(\delta, \Delta t, \Delta\Phi, q) = [(2\Delta\Phi)^2 + q^2]^{1/2}\sin\left(\frac{2\delta\Delta t}{3} - \theta\right), \tag{14c}$$

where

$$\tan\theta = \frac{q}{2\Delta\Phi}. \tag{14d}$$

The envelope function $f(\delta, \tau, \Delta t)$ comprises the frequency-detuning-dependent amplitude $\exp(\delta^2\tau^2/6)$ and the time-delay-dependent Gaussian function $\exp(-2\Delta t^2/3\tau^2)$. This Gaussian dependence is a result of the frequency-domain third-order autocorrelation $A(\Delta t, \omega)[=\int_{-\infty}^{\infty}E(t - \Delta t)|E(t)|^2\exp(-i\omega t)dt]$ performed in the measurement. The amplitude part, on the other hand, reflects the dependence of the frequency detuning on the signal strength in the nonlinear transmittance measurements. With the detection at a wavelength away from the central wavelength of the probe beam, the relative variation of the signal strength induced by the probe beam with respect to the original probe signal is larger. This is so because the unperturbed probe signal at a larger frequency detuning is smaller with the same amount perturbation by the pump beam. In Fig. 1(a) we demonstrate the dependence of frequency shift δ on the envelope function, based on Eq. (14b). Here $\Delta\Phi = 3.8 \times 10^{-4}$ rad and τ is 85 fs. As is shown in this figure, the larger the frequency detuning is, the larger the envelope function is. Furthermore, according to Eq. (14b), the amplitude part depends on the absolute value of δ, not on its sign.

The origin of the modulation function $\zeta(\delta, \Delta t, \Delta\Phi, q)$ can easily be illustrated first for the condition of absence of two-photon absorption ($q = 0$). For the chirp-free laser pulses, $E_{\mathrm{pr}}(z = 0, t)$ and $\Delta E_{\mathrm{pr}}(z = L, t)$ can be written as

$$E_{\mathrm{pr}}(z = 0, t) = E_{\mathrm{pr}}{}^0\exp(-t^2/\tau^2)\exp(i\omega_0 t), \tag{15a}$$

$$\begin{aligned}\Delta E_{\mathrm{pr}}(z = L, t) &= E_{\mathrm{pr}}{}^0(i2\Delta\Phi + q)\\ &\quad\times\exp\left[-\frac{2(\Delta t)^2}{3\tau^2}\right]\exp\left[-\frac{3}{\tau^2}\left(t + \frac{2}{3}\Delta t\right)^2\right]\\ &\quad\times\exp(i\omega_0 t)\\ &= E_{\mathrm{pr}}{}^0(i2\Delta\Phi + q)\\ &\quad\times\exp\left[-\frac{2(\Delta t)^2}{3\tau^2}\right]\exp\left(-\frac{3}{\tau^2}t'^2\right)\\ &\quad\times\exp(i\omega_0 t')\exp\left(-i\frac{2\omega_0\Delta t}{3}\right),\end{aligned} \tag{15b}$$

where $t' = t + 2\Delta t/3$. Comparing the time dependences of these two electric fields, we see a time shift $2\Delta t/3$ between their envelope functions. Furthermore, Eq. (15b) indicates that there is a phase shift $\exp(-i2\omega_0\Delta t/3)$ in the carrier wave with respect to the center of the envelope function. When the change in the transmitted probe intensity is detected, the interference between $E_{\mathrm{pr}}(z = 0, t)$ and $\Delta E_{\mathrm{pr}}(z = L, t)$ is in effect monitored. After the monochromator, only a specific frequency component of the probe beam is selected, yielding a phase shift $\exp(i2\omega\Delta t/3)$ at $\Delta E_{\mathrm{pr}}(z = L, t)$. The total phase shift is therefore equal to $\exp[i2(\omega - \omega_0)\Delta t/3] = \exp(i2\delta\Delta t/3)$. It is this phase shift between $E_{\mathrm{pr}}(z = 0, t)$ and $\Delta E_{\mathrm{pr}}(z = L, t)$ that leads to the modulation function in Eq. (5). Figure 1(b) shows the change in normalized transmittance as a function of the pump–probe time delay for different frequency detunings. It displays an antisymmetric oscillatory behavior, and the different δ values vary only the signal amplitude not the oscillatory feature. With two-photon absorption ($q \neq 0$), it in effect induces

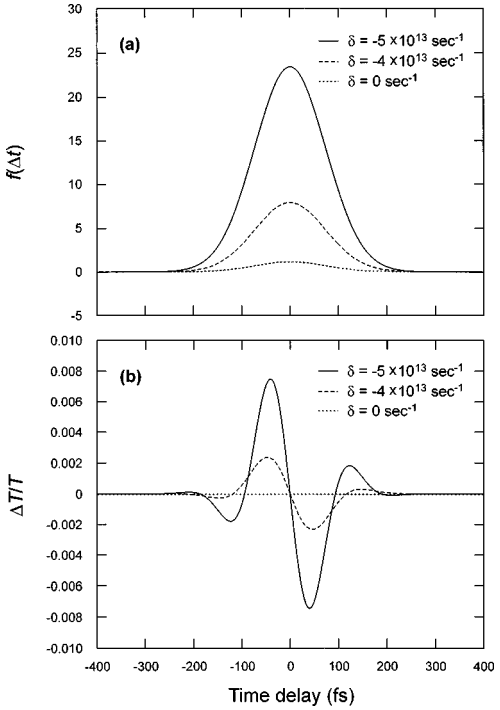

Fig. 1. Simulated nonlinear transmittance transients with the chirp-free model at three frequency detunings δ. (a) Envelope function $f(\Delta t)$, (b) total transient signal. The induced phase shift $\Delta\Phi$ is 4×10^{-4} rad.

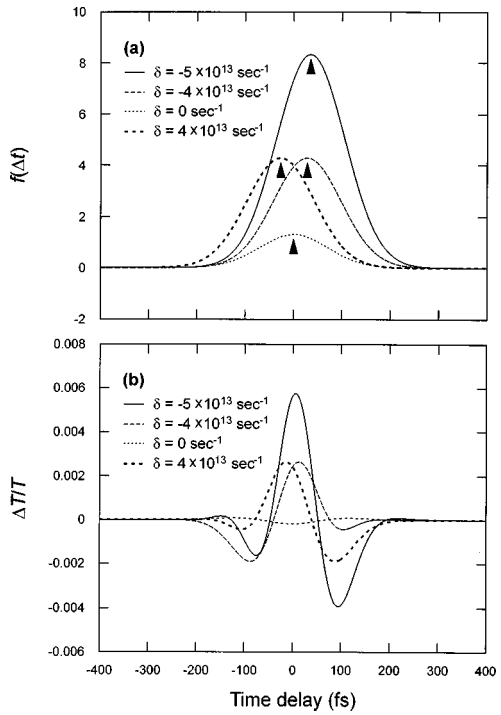

Fig. 2. Simulated nonlinear transmittance transients with the linear-chirp model at three frequency detunings δ. (a) Envelope function $f(\Delta t)$, (b) total transient signal. Arrows denote the peak positions of $f(\Delta t)$. $b = 9 \times 10^{25}\,\mathrm{s}^{-2}$, $\Delta\Phi = 3.8 \times 10^{-4}$ rad.

an imaginary phase in the probe beam. This time-delay-dependent imaginary phase and the real phase caused by $\Delta\Phi$ lead to a complex constant $i2\Delta\Phi + q$ in $\Delta E_{\mathrm{pr}}(L, \omega)$. This complex constant thus induces a constant phase shift in the modulation function.

B. Linear-Chirp Model

For the linearly chirped Gaussian pulses used in the two-beam coupling measurements, Equations (11) provide an analytical expression for the transmitted probe beam at a frequency detuning δ. In this subsection we calculate the results of this equation with different parameters. We choose the material parameters of fused silica in the calculation as $L = 2\,\mathrm{mm}$, $n_2{}^I = 2.2 \times 10^{-20}\,\mathrm{m}^2/\mathrm{W}$, $n_0 = 1.45332$, and $\beta = 0$. Furthermore, the peak intensity of the pump pulse is $10^{12}\,\mathrm{W/m}^2$, the central wavelength is 793 nm, and $\tau = 85\,\mathrm{fs}$. These laser parameters are chosen to be close to our experimental conditions.

Similar to Eq. (5), Eq. (11a) can be regarded as the product of an envelope function,

$$f(\Delta t) = h(b, \tau)\exp[g(b, \delta, \tau)] \times \exp\{-[\Delta t - T_s(b, \delta, \tau)]^2/[\Gamma(b, \tau)]^2\}, \tag{16}$$

where $h(b, \tau)$ is the amplitude in Eq. (11a) with a modulation function

$$2\Delta\Phi \sin\Theta - q\cos\Theta. \tag{17}$$

Figure 2 shows the calculation results at two frequency-detuning values for $b = 9 \times 10^{25}\,\mathrm{s}^{-2}$. In comparison with the chirp-free results, the increase here in the negative frequency detuning shifts the peak of the envelope function toward the positive time-delay position for a positive chirp [Fig. 2(a)]. The positive frequency detuning, on the other hand, shifts the envelope function to the negative time delay. This feature is evidenced by the linear dependence of $T_s(b, \delta, \tau)$ on δ in Eq. (11b). The positive b represents that the low-frequency component of the laser pulse is ahead of the high-frequency component. Because the low-frequency component of the probe pulse is shifted to the rising edge, the effective peak position in time of the probe pulse for $\delta < 0$ is then moved to an earlier time with respect to the original pulse. From Eqs. (11), the normalized transmittance signal is therefore largest when the pump pulse is situated at the rising edge of the probe pulse, namely, at the positive time delay, where the maximum temporal overlap between the pump pulse and the effective probe pulse appears. Apparently, the larger the positive chirp is, the more the peak position of the signal is shifted toward the positive time delay.

As in the discussion of the case without chirp, the change in the linearly chirped probe field after interaction with the pump beam in the sample can be written as

$$\Delta E_{\mathrm{pr}}(z = L, t) = E_{\mathrm{pr}}{}^0(i2\Delta\Phi + q)\exp\left[-\frac{2(\Delta t)^2}{3\tau^2}\right] \times \exp\left(-\frac{3}{\tau^2}t'^2\right)\exp(i\omega_0 t')\exp(ibt'^2) \times \exp\left(-i\frac{2\omega_0\Delta t}{3}\right) \times \exp\left\{-ib\left[\frac{4\Delta t}{3}t + \frac{4}{9}(\Delta t)^2\right]\right\}, \tag{18}$$

where $t' = t + 2\Delta t/3$. The total phase shift between $E_{\mathrm{pr}}(z = 0, t)$ and $\Delta E_{\mathrm{pr}}(z = L, t)$ after the monochromator is therefore equal to

$$\exp\left(i\frac{2\delta\Delta t}{3}\right)\exp\left\{-ib\left[\frac{4\Delta t}{3}t + \frac{4}{9}(\Delta t)^2\right]\right\}.$$

Note that it does not disappear, even when $\delta = 0$, which is the opposite of the case without chirp, as shown in Fig. 2(b). Furthermore, the second-order time dependence in the phase from the linear chirp leads to the second-order dependence on Δt in the total phase shift, yielding a nonlinear period in the modulation function, as shown in Eqs. (11) and Fig. 2(b). In comparison with the chirp-free case [Fig. 1(b)], the transient signal in Fig. 2(b) would not necessarily reach zero at $\Delta t = 0$, and the oscillatory feature depends on the δ value.

Finally, a discussion of the effect of the linear chirp parameter b is given below. Both the envelope function and the total nonlinear transmittance were calculated with three positive linear chirp parameters: 0, 5×10^{25}, and $9 \times 10^{25}\,\mathrm{s}^{-2}$. The larger the positive chirp is, the more the low-frequency component is shifted to the rising edge of the laser pulse, yielding a larger time shift in the peak position, as shown in Fig. 3(a). Notice that the larger b is, the smaller the envelope function $f(\Delta t)$ is. When linear chirp parameter b is involved in the frequency-domain third-order autocorrelation $A(\Delta t, \omega)$, the linear

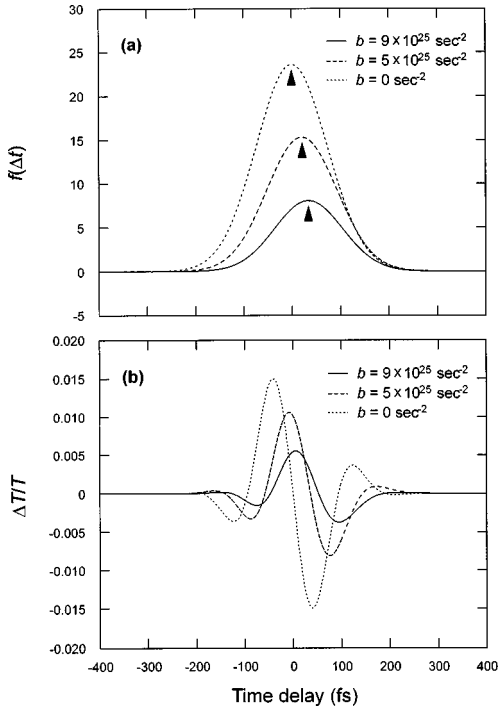

Fig. 3. Simulated nonlinear transmittance transients with the linear-chirp model for three linear chirp parameters b. (a) Envelope function $f(\Delta t)$, (b) total transient signal. Arrows denote the peak positions of $f(\Delta t)$. $\delta = -5 \times 10^{13}\,\mathrm{s}^{-1}$; $\Delta\Phi = 3.8 \times 10^{-4}$ rad.

chirp creates a larger spectral broadening in $A(\Delta t, \omega)$ than the initial linearly chirped probe pulse. This spectral broadening decreases the normalized transmittance signal with a specific spectral window for detection. Because of the combination of linear chirp and frequency detuning, the total transient feature exhibits a nonsymmetrical modulation feature, as shown in Fig. 3(b).

4. EXPERIMENT

Figure 4 shows a schematic layout of the experimental setup. The output of a femtosecond mode-locked Ti:sapphire laser (Tsunami, Spectra-Physics) served as the pulsed light source for both the pump and the probe beams. We can fine tune the chirp by adjusting the position of one of four dispersion-compensated prisms inside the cavity. A total average power of ~250 mW was used in the experiment. The central wavelength of the output beam was ~793 nm. In performing the pump–probe transmittance measurements we split the output of the femtosecond Ti:sapphire oscillator with a 90/10 (reflection/transmission) beam splitter into pump and probe beams. The beam passing through mirrors M1–M3 is the probe beam, and the one passing through mirrors M4–M7 is the pump beam. A computer-controlled translation stage was used to vary the time delay between the pump and the probe pulses with a resolution of 0.1 μm. The pump and probe beams were then focused noncollinearly into the sample by a plano–convex lens ($f = 11.4$ cm). To minimize the time-delay error that is due to the noncollinear overlap between the pump and the probe pulses at the sample we selected the separation between the two parallel pump and probe beams to be ~5 mm, which resulted in a crossing angle of ~2.5° between the pump and probe beams. The transmitted probe beam then went to a 27-cm monochromator that selected a specific detecting wavelength with a spectral width of ~0.2 nm. A photomultiplier (R928, Hamamatsu) detected the filtered laser's intensity after the monochromator as a function of the pump–probe time delay. A chopper was placed in the path of the pump beam for phase lock-in detection, as shown in Fig. 4. We carried out the measurements by accumulating and averaging 50–60 fast time-delay scans.

A 500-μm-thick β-barium borate crystal was substituted into the sample for an *in situ* second-harmonic generation (SHG) autocorrelation measurement to determine time zero as well as the pulse duration. The autocorrelation trace is shown in Fig. 5(a). The extracted pulse duration (full width at half-maximum) is 100 fs, corresponding to a pulse-width parameter of 86.6 fs for a Gaussian pulse. The spectrum of the laser pulse was measured with a spectrometer system and is shown in Fig. 5(b). Assuming a linearly chirped Gaussian pulse, the chirp parameter is calculated to be $1.0 \times 10^{26}\,\mathrm{s}^{-2}$. We measured the power density of the pump pulse at the sample by scanning a 5 μm-diameter pinhole across the focal spot of the pump beam. The beam waist diameters at the focal point were 78 and 108 μm along x and y axes, respectively, of the beam's cross section. Assuming a Gaussian beam, the corresponding confocal parameters are 12 and 23 mm, respectively. The peak pump power density at the beam waist was estimated to be $\sim 10^{12}\,\mathrm{W/m}^2$. Because the pump and probe beams intersect at the sample with a crossing angle of ~2.5°, the actual power density may be different from this value. Finally, we fitted the nonlinear transmittance transients of the probe beam at several frequency detunings by a nonlinear least-squares fitting program (Origin 5.0, Microcal) to extract the induced phase shift as well as the linear chirp in the laser pulses.

To measure the complex time-varying electric field $E(t)$ we installed a SHG FROG setup to perform the measurements. The setup is similar to the one used by Taft *et al.*[5] A 200 μm type I KDP frequency-doubling crystal was chosen to minimize the GVD. Its corresponding phase-matching bandwidth was calculated to be ~60 nm, which should provide enough bandwidth for the SHG pro-

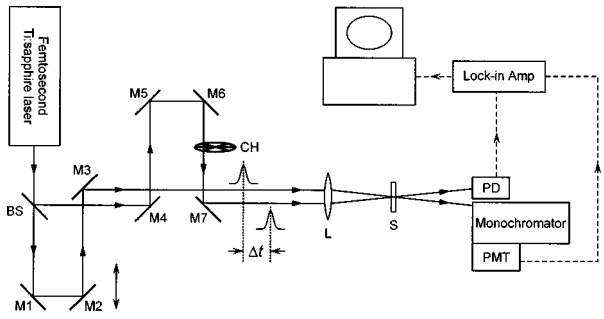

Fig. 4. Experimental layout for the transient nonlinear transmittance measurements. Mirrors M1–M7 are Ag coated. BS, beam splitter (reflection/transmission, 90/10); CH, chopper; L, plano–convex lens ($f = 11.4$ cm); S, sample; PD, photodiode detector; PMT, photomultiplier tube.

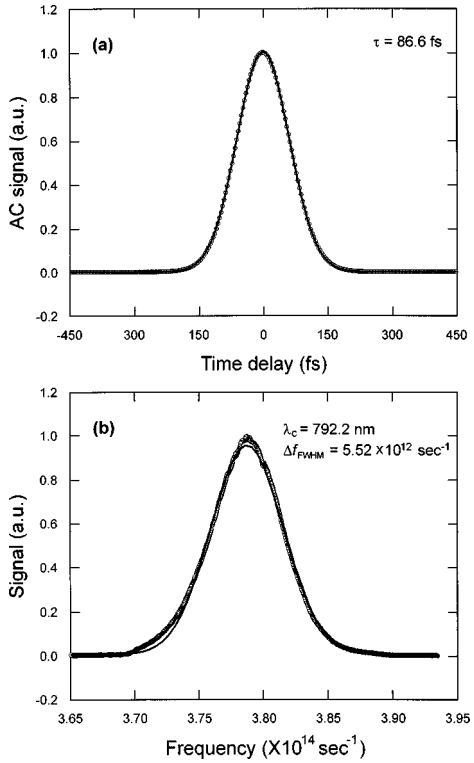

Fig. 5. Autocorrelation trace and spectrum of the femtosecond laser pulses at the output of the mode-locked Ti:sapphire oscillator. Solid curves, Gaussian fitting curves. The fitted pulse-width parameter is τ, and the full width at half-maximum Δf_{FWHM} of the laser spectrum in frequency is shown ($\Delta\lambda_{\mathrm{FWHM}} = 11.5$ nm).

cess. Furthermore, except for the 50/50 beam splitter of femtosecond laser pulses, all the optics are Ag-coated mirrors to prevent any residual dispersion effect. The crossing angle at the crystal between the two beams was chosen to be ~3° to minimize the time-delay error that was due to the noncollinear overlap between the pump and the probe pulses. The output SHG signal was then dispersed by a spectrometer (270M, ISA) and detected by a photodiode array. The spectrometer system monitored the SHG spectrum as a function of the time delay between the two beams, leading to a FROG trace. The FROG trace was measured with a time step of 6.6 fs and a spectral resolution of 0.1 nm and was subsequently analyzed with a phase-retrieval program (FROG 2.0, Femtosoft Technologies).

5. RESULTS AND DISCUSSION

A. Model System: Fused Silica

Fused silica is an ideal optical material for many applications. Many of its linear optical properties are well characterized and documented. Fused silica has commonly been used as a window material for high-power lasers and is the basic material for soliton-based long-haul fiber optical communication, which relies on its third-order optical nonlinearity. The nonlinear refractive index of fused silica has been determined by many research groups and has recently been reviewed.[6] We thus use this material as our model system to check the validity of our linear chirp model and to help us to understand the effects of higher-order chirps.

Figure 6 shows the normalized transmittance transient on the 2-mm fused-silica sample for femtosecond laser pulses at two detection wavelengths (781.5 and 806.5 nm). The purpose for performing measurements at these two wavelengths was to demonstrate the difference in the transients caused by the chirp and to check the validity of the linear chirp model at different frequency detunings. To compare these experimental data with the simulation results based on the complete-chirp model we extracted the electric-field amplitude and phase of the laser pulses from the SHG FROG trace. Figure 7 shows the FROG spectrogram and the corresponding intensity and phase. Figure 8 shows the corresponding simulation results with comparable laser and material parameters, except that the complete phase obtained from the FROG measurement was used in the calculation.[7] As Figs. 6 and 8 show, at each detection wavelength the experimental and simulation transients have nearly the same major features, with only slight differences. This result demonstrates that the theoretical calculation with the complete chirp can reproduce the experimental results; it has thus been proved to be a helpful tool for studying the two-beam coupling process.[8]

We performed the fitting with the linear chirp model on both the experimental and the simulation results (Figs. 6 and 8), with all the parameters independently optimized. The corresponding fitted results are listed in Tables 1 and 2. Because the bandgap for fused silica (>4.4 eV) is more than twice the photon energy of the laser pulses (1.55 eV),

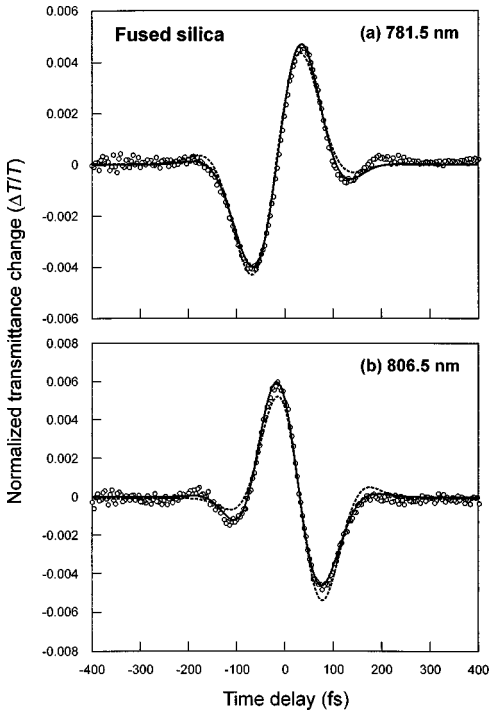

Fig. 6. Normalized nonlinear transmittance signals obtained for 2-mm-thick fused silica at two detection wavelengths. Open circles, experimental data; solid curves, best-fitting curves with the linear-chirp model. Their fitted results are listed in Table 1. Dashed curves, fitting curves for the chirp-free model.

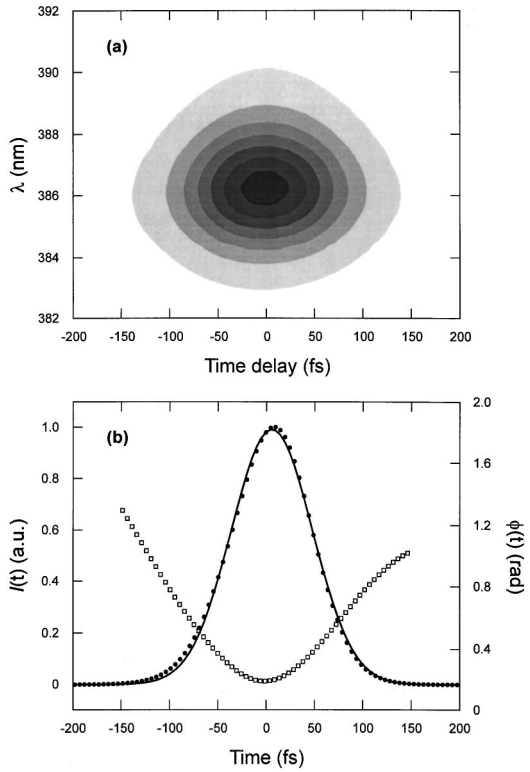

Fig. 7. Intensity and phase data of the laser pulses extracted from the SHG FROG spectrograms. (a) FROG spectrogram, (b) corresponding intensity $I(t)$ and phase $\phi(t)$. Filled circles, intensity data; open squares, phase data. Solid curve, the best Gaussian fit to the intensity. The fitted pulse-width parameter is 84.2 fs.

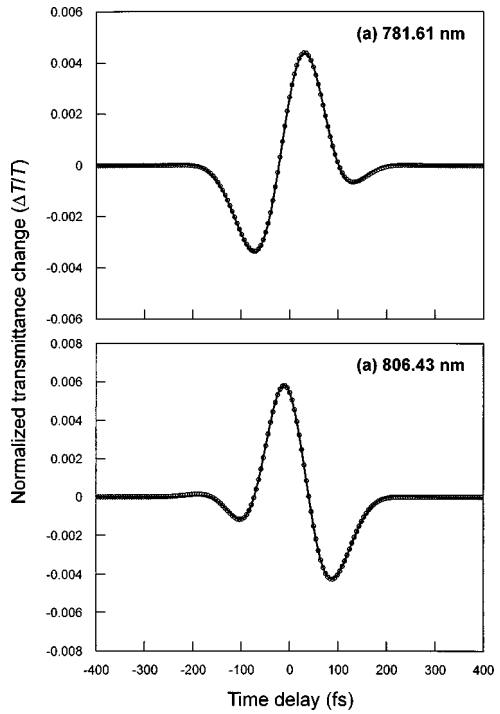

Fig. 8. Simulated results for the normalized nonlinear transmittance measurements at two detection wavelengths. The chirp was obtained by the FROG trace (described in text). Open circles, simulation data; solid curves, the fitting curves with the linear-chirp model. Fitting results are listed in Table 2.

Table 1. Results Obtained by Fitting the Experimental Data on 2-mm Fused Silica with the Linear-Chirp Model[a]

	Detection Wavelength (nm)	
Parameter	781.5	806.5
$\Delta\Phi$ (10^{-3} rad)	0.62 ± 0.04	0.52 ± 0.03
b (10^{25} s^{-2})	3.6 ± 0.3	5.7 ± 0.4
δ (10^{13} s^{-1})	3.61 ± 0.03 (3.538)	−4.26 ± 0.03 (−4.017)
τ (fs)	84.0 ± 1.1	83.6 ± 0.9
t_0 (fs)	6.9 ± 1.3	0.9 ± 1.5
χ^2 (10^{-8})	2.63	3.4

[a] $\Delta\Phi$ is the phase shift, b is the linear chirp, δ is the frequency detuning, τ is the pulse-width parameter, t_0 is the time shift, and χ^2 is the fitting error. The numbers in parentheses are the measured values.

Table 2. Results Obtained by Fitting the Simulated Transients at Two Frequency Detunings[a]

	Detection Wavelength (nm)	
Parameter	781.61	806.43
$\Delta\Phi$ (10^{-3} rad)	0.584 ± 0.004	0.620 ± 0.004
b (10^{25} s^{-2})	5.74 ± 0.04	7.30 ± 0.05
δ (10^{13} s^{-1})	3.655 ± 0.003 (3.462)	−4.140 ± 0.004 (−3.956)
τ (fs)	88.2 ± 0.1	86.9 ± 0.1
t_0 (fs)	8.2 ± 0.2	−0.2 ± 0.2
χ^2 (10^{-10})	1.58	2.78

[a] $\Delta\Phi$ is the phase shift, b is the linear chirp, δ is the frequency detuning, τ is the pulse-width parameter, t_0 is the time zero, and χ^2 is the fitting error. The numbers in parentheses are the values used in the calculation.

the two-photon absorption effect was then neglected in the fitting. For the two detection wavelengths, both the time zero positions and the pulse-width parameters τ obtained were all within a variation of ±10 fs imposed by the error in the computer-controlled translation stage. We also performed the fitting with the chirp-free model [Eq. (5)] at the two frequency detunings (as shown in Fig. 6). For the detected probe wavelength at 781.5 nm, the extracted $\Delta\Phi$ is 5.7×10^{-4} rad and χ^2 is 4.2×10^{-8}; for 806.5 nm, the extracted $\Delta\Phi$ is 4.9×10^{-4} rad and χ^2 is 9.6×10^{-8}. Notice that neither of the fittings is satisfactory and that the extracted $\Delta\Phi$ values differ from those obtained with the linear-chirp model. The extracted linear chirp values, however, differ by >50% for the experimental results and by <20% for the simulation results. This result can be explained by the fact that the higher-order chirps are not considered in the linear-chirp model. The fitted linear chirp b can then be understood as an effective linear chirp under the influence of other higher-order chirps. This is why the fitted b varies for the two different detection wavelengths. Finally, the deduced phase shift, $\Delta\Phi$, varies less 20% for the two frequency detunings, indicating that $n_2{}^I$ extracted by this method may cause only a small amount of error.

To extract the nonlinear optical constants from $\Delta\Phi$ and q one has to determine the interaction length L accu-

rately. It may not be the same as the sample thickness and depends on the crossing angle between the pump and the probe beams. Because the confocal parameters for the x and the y axes are 12 and 23 mm, respectively, which are much longer than the thickness of our samples, the divergence of the laser beam can be ignored. Because the phase induced by the pump pulse is very small ($<10^{-3}$ rad) here, the change in the beam propagation properties of the pump and probe beams is then negligible. We can approximate the crossing between two Gaussian beams,

$$I(x, y) = I_0 \exp(-x^2/\sigma_x{}^2)\exp(-y^2/\sigma_y{}^2),$$

as the crossing between two flat-topped beams with beam diameters equal to $2\sigma_x$ in the x direction and to $2\sigma_y$ in the y direction. We therefore ignore the effect of the radius dependence of the laser intensity across the beam profile. Along the direction between the propagation directions of the two beams (z axis), the overlap cross-section area of the two beams can be written as $A(z)$. The effective induced phase shift at a z position for a sample thickness of δz is then given by

$$\Delta\phi(z) = -\frac{\omega_0}{c} n_2{}^I \frac{A(z)}{A_0} I_{\mathrm{pu}}{}^0 \delta z, \tag{19}$$

where A_0 is the maximum overlap area. The total induced phase shift is thus the integration over the whole interaction region, i.e.,

$$\Delta\phi_{\mathrm{total}} = -\frac{\omega_0}{cA_0} n_2{}^I I_{\mathrm{pu}}{}^0 \int_{z_0-L/2}^{z_0+L/2} A(z)\mathrm{d}z, \tag{20}$$

where z_0 is the middle position of the sample. The integration in Eq. (19) is effectively equal to the total intersection volume between the two laser beams. This volume divided by the cross-section area of the laser beam at the focal point is then equal to the effective interaction length. Its calculated value is 0.76 mm for our experimental setup. Thus for our fused-silica sample the actual interaction length should be equal to 0.76 mm instead of to the sample thickness. Similarly, in extracting the two-photon absorption coefficient one should also apply the same considerations.

Because the only material parameter that influences the normalized transmittance transient in the two-beam coupling measurement is $n_2{}^I$, fused silica can be used as a reference material for extraction of the nonlinear refractive indices of other materials. During the experiment one can a first measure the transmittance transient data by using a fused-silica sample with a well-defined thickness. With the same experimental setup, the new sample can then be inserted into the same sample position for the measurement. The two measured transients should be identical. After the ratio of the pump laser powers inside the two samples is taken into account, the ratio between their nonlinear refractive indices can then be determined by the ratio in their nonlinear transmittance data.

FROG was recently used successfully for extraction of $n_2{}^I$ in several optical materials. In a single-beam experiment the phase difference $\Delta\phi(t)$ caused by self-phase modulation was calculated by extraction of the electric-field phase before and after it interacted with the sample.[9] In a pump–probe experiment, $\Delta\phi(t)$ caused by cross-phase modulation from the pump pulse was derived by extraction of the electric-field phase of the probe pulse with and without interaction with the pump pulse in the sample.[10] This use of FROG to measure the phase change, however, has two limitations. First, it requires a higher laser power density ($>10^{13}$ W/m^2) to induce enough phase difference ($>10^{-2}$ rad) for complete phase retrieval. In comparison, the transient nonlinear transmittance technique described in this paper can reach a sensitivity of $<10^{-6}$ rad with a power density of only $<10^9$ W/m^2. Second, applying the phase retrieval algorithm in calculating the complete phase permits no two-photon absorption effect in the nonlinear interaction between the laser pulse and the material. Thus the use of this technique is restricted to media with large energy bandgaps, such as fused silica and wide-bandgap semiconductors. The transient nonlinear transmittance technique, however, has the capability to extract $n_2{}^I$ and β simultaneously, as we demonstrate below.

B. $n_2{}^I$ and β of Semiconductor-Doped Glasses

To illustrate their capability to measure two-photon absorption coefficient β, we selected two kinds of semiconductor-doped glass (OG550 and RG610) with which to perform the experiment. Semiconductor-doped glasses are manufactured by addition of the semiconductor constituents or their oxides to the silicate glass melt.[11] In the cooling stage, the semiconductor material is then precipitated into nanocrystals. The electronic levels of these semiconductor nanocrystals are affected by their size because of the quantum-confined effect.[12] One can thus finely adjust the optical properties by varying the sizes of these nanocrystals during the growth process. These semiconductor-doped glasses are commonly used as colored glass filters and also have many potential nonlinear optical applications. Tuning the electronic states of the embedded nanocrystals close to the resonant condition can thus enhance the third-order optical nonlinearities by many orders of magnitude.

The doping semiconductor material for OG550 and RG610 is CdS_xSe_{1-x}. The difference between these materials lies in the average radius of the precipitated nanocrystals. The one-photon absorption threshold of OG550 is 2.25 eV, and that of RG610 is 2.03 eV.[13] With the laser wavelength at ~800 nm (1.55 eV), the two-photon absorption effect is then involved in the two-beam coupling measurement. The samples can then be used as the testing materials for the measurement. The thickness of both samples is 3 mm. Figure 9 shows the experimental results for RG610 at 781.5 nm. The results fitted with the linear-chirp model are listed in Table 3. To extract $n_2{}^I$ and β accurately we performed the experiment on fused silica at the same time. The ratio value of the fitted phase shift in RG610 and the corresponding one in fused silica is 2.425. The interaction length of 0.76 mm was then used in the calculation. The resultant $n_2{}^I$ is equal to 5.8×10^{-20} m^2/W, which is comparable with the previously published result at 1.064 μm (6.2×10^{-20} m^2/W).[11,13] We used this number to obtain the effective laser intensity $I_{\mathrm{pu}} = 2.5 \times 10^{12}$ W/m^2 in the

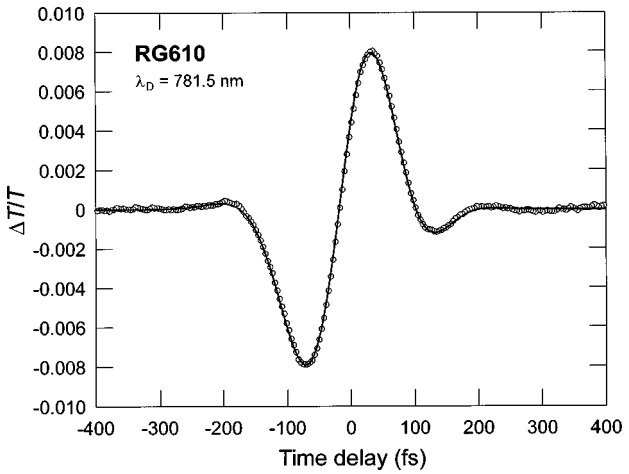

Fig. 9. Normalized nonlinear transmittance signal obtained for 3-mm RG610 semiconductor-doped glass at 781.5 nm. Open circles, experimental data; solid curve, fitting curve with the linear-chirp model. Fitting results are listed in Table 3.

Table 3. Results Obtained by Fitting the Experimental data at 781.5 nm on 3-mm Semiconductor-Doped Glasses with the Linear-Chirp Model[a]

	Glass	
Parameter	RG610	OG550
$\Delta\Phi$ (10^{-3} rad)	0.88 ± 0.02	1.22 ± 0.03
q (10^{-3})	0.61 ± 0.01	1.22 ± 0.01
b (10^{25} s^{-2})	5.05 ± 0.09	4.56 ± 0.08
δ (10^{13} s^{-1})	3.73 ± 0.01 (3.538)	3.45 ± 0.01 (3.538)
τ (fs)	91.4 ± 0.3	91.7 ± 0.4
χ^2 (10^{-8})	0.68	0.86

[a] $\Delta\Phi$ is the phase shift, b is the linear chirp, δ is the frequency detuning, τ is the pulse-width parameter, and χ^2 is the fitting error. The numbers in parentheses are the measured values.

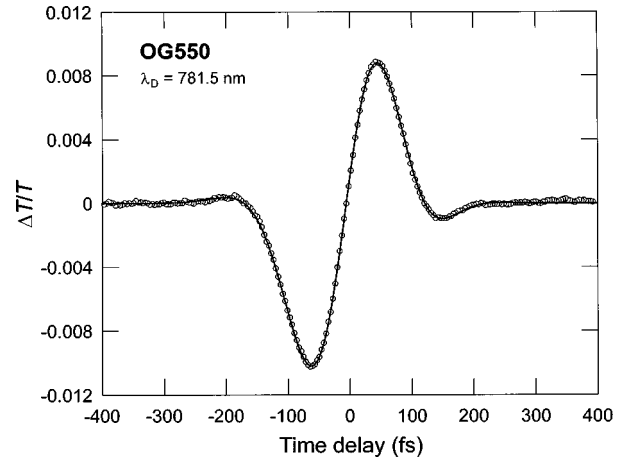

Fig. 10. Normalized nonlinear transmittance signal obtained for 3-mm OG550 semiconductor-doped glass at 781.5 nm. Open circles, experimental data; solid curve, fitting curves with the linear-chirp model. Fitting results are listed in Table 3.

measurement. We could then obtain the two-photon absorption coefficient by dividing the fitted q value by the effective pump intensity and the interaction length. The resultant β is 3.2×10^{-13} m/W, which is very close to the reported value at the same wavelength (2.2×10^{-13} m/W).[11] The experimental results for OG550 at 781.5 nm are shown in Fig. 10. The corresponding fitted results are shown in Table 3. From the same characterization approach, the extracted value of n_2^I is 8.1×10^{-20} m^2/W, and the β value is 6.4×10^{-13} m/W. We believe that this is the first time that the two nonlinear optical constants of the OG550 glass have been measured.

6. CONCLUSIONS

The nonlinear transient transmittance measurement with femtosecond laser pulses is a highly sensitive method for extracting the nonlinear optical constants n_2^I and β. The chirp-free model has provided a convenient formula to explain the transient features measured by transform-limited femtosecond laser pulses. The commonly found chirp in ultrashort laser pulses has, however, inhibited the use of chirped laser pulses in measuring n_2^I and β based on the chirp-free model. We have derived a generalized model to explain analytically the transient behavior observed in linearly chirped femtosecond laser pulses. This linear-chirp model has thus successfully provided an intuitive language for understanding the major effects caused by the linear chirp embedded in ultrashort laser pulses. The analytical formula thus derived can be regarded as the product of two parts: the envelope function and the modulation function. The envelope function is a Gaussian function with a time shift that depends on the linear chirp parameter. Furthermore, the modulation function can be understood as a nonlinear phase interference caused by the linear chirp.

We have performed two-beam coupling experiments, using chirped femtosecond laser pulses on fused silica. The experimental data can be well fitted by the linear-chirp model. The complete intensity and phase information obtained from the FROG measurement was used to simulate the transient transmittance signals. The close match between the experimental and simulation results has confirmed that our simulation based on the complete-chirp model can reproduce the experimental results. We also performed nonlinear transient transmittance measurements of semiconductor-doped glasses to extract their nonlinear optical constants. We used the experimental result for fused silica as a reference system to determine these constants accurately.

Finally, based on our linear-chirp model, the two-beam coupling method can potentially serve as a monitoring system to measure the linear chirp embedded in the output of ultrafast laser systems. This technique is much simpler than other, more-complex phase retrieval techniques, such as FROG, because it does not involve elongated calculation and the experimental setup is much simpler. Therefore our new technique not only provides a new method for measuring nonlinear optical constants by use of chirped laser pulses but also offers a new tool for monitoring chirp. The chirp in the laser pulses can easily be reflected in the asymmetrical feature in the nonlinear transmittance transient. A real-time monitoring apparatus that uses the spectrally resolved two-beam coupling method would therefore provide a convenient tool for adjusting the dispersion-compensation element in

femtosecond laser systems (such as the prism position for mode-locked oscillators and the grating separation in the compressor of ultrafast regenerative amplifiers). We intend to implement this technique to retrieve and monitor chirp in real time at the output of a femtosecond laser system.

ACKNOWLEDGMENTS

This research was supported by the National Science Council (grants nos. NSC 88-2112-M-002-026 and 88-2112-M-001-038) of Taiwan.

J.-K. Wang's e-mail address is jkwang@ccms.ntu.edu.tw.

REFERENCES AND NOTES

1. R. L. Sutherland, *Handbook of Nonlinear Optics* (Marcel Dekker, New York 1996), and references therein.
2. M. Sheik-Bahae, A. A. Said, T.-H. Wei, D. J. Hagan, and E. W. Van Stryland, IEEE J. Quantum Electron. **QE-6**, 760 (1990), and references therein.
3. X. Kang, T. Krauss, and F. Wise, Opt. Lett. **22**, 1077 (1997).
4. J.-C. Diels and W. Rudolph, *Ultrashort Laser Pulse Phenomena* (Academic, San Diego, Calif. 1995).
5. G. Taft, A. Rundquist, M. Murnane, I. P. Christov, H. C. Kapteyn, K. W. DeLong, D. N. Fittinghoff, M. A. Krumbügel, J. N. Sweetser, and R. Trebino, IEEE J. Sel. Top. Quantum Electron. **2**, 575 (1996).
6. D. Milam, Appl. Opt. **37**, 546 (1998).
7. In the calculation of the simulated nonlinear transmittance signals we used the complete phase derived from the FROG measurement. The best Gaussian fit to the intensity data was adopted in the calculation. A calculation with the actual intensity data was also performed, which resulted in a worse match with the experimental nonlinear transmittance data, perhaps because of an error in the intensity retrieved from the FROG measurement.
8. We also performed the calculation by using different orders of polynomials to fit the extracted phase from the FROG measurement. We found that the amplitude of the simulated transient when only the linear chirp was used did not agree with the experimental data. When the higher-order chirps were included in the calculation, the whole body of experimental data could be reproduced. A close comparison of the experimental and the simulation results has shown that there are still slight differences between them. Furthermore, the sample length is one hundredth of the dispersion length L_D. The effect of GVD is normally regarded to be negligible [G. P. Agrawal, *Nonlinear Fiber Optics*, 2nd ed. (Academic, San Diego, Calif. 1989), Chapter 4]. It is thus conceivable that this discrepancy is due to errors in intensity and phase of the laser pulses extracted from the FROG measurement. This fact has further demonstrated that the transient nonlinear transmittance technique is more sensitive to the chirp than is FROG.
9. A. J. Taylor, G. Rodriguez, and T. S. Clement, Opt. Lett. **21**, 1812 (1996).
10. G. Rodriguez and A. J. Taylor, Opt. Lett. **23**, 858 (1998).
11. G. P. Banfi, V. Degiorgio, and D. Ricard, Adv. Phys. **47**, 447 (1998).
12. M. G. Bawendi, M. L. Steigerwald, and L. E. Brus, Annu. Rev. Phys. Chem. **41**, 477 (1990); Y. Wang and N. Herron, J. Phys. Chem. **95**, 525 (1991); A. P. Alivisatos, J. Phys. Chem. **100**, 13,226 (1996); A. Tomasulo and M. C. Ramakrishna, J. Chem. Phys. **105**, 3612 (1996).
13. G. P. Banfi, V. Degiorgio, D. Fortusini, and H. M. Tan, Appl. Phys. Lett. **67**, 13 (1995).